ACS APPLIED MATERIALS & INTERFACES

Research Article

www.acsami.org

Photoelectrochemical Hydrogen Production of TiO_2 Passivated Pt/Si-Nanowire Composite Photocathode

Shipu Li, Peng Zhang,* Xuefeng Song, and Lian Gao*

State Key Lab of Metal Matrix Composites, School of Materials Science and Engineering, Shanghai Jiao Tong University, Shanghai, 200240, China

Supporting Information

ABSTRACT: Si nanowire (SiNW) arrays decorated with Pt nanoparticles are passivated with TiO_2 surface layer using atomic layer deposition (ALD). The sandwich structure TiO_2/Pt/SiNW shows superior photoelectrochemical performance to the control planar silicon electrodes, especially under the concentrated solar radiation. Pt nanoparticles separated from aqueous electrolyte by TiO_2 layer of more than 15 nm still well catalyze surface photoelectrochemical hydrogen production without direct contact to the electrolyte. This structural configuration shows remarkable chemical stability and anodically shifted onset potential, suggesting great promise for applications in solar hydrogen production. The maximum photon-to-energy conversion efficiency of the TiO_2/Pt/SiNW reaches 15.6%.

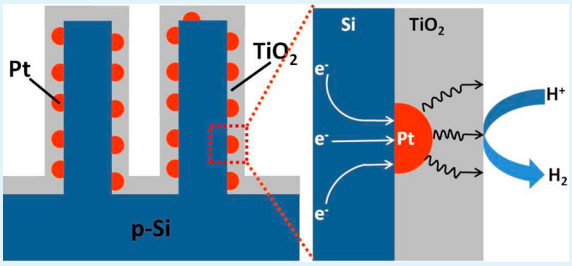

KEYWORDS: *Si nanowire arrays, TiO_2, passivation, ALD, photoelectrochemical, hydrogen*

INTRODUCTION

The increasing demand for clean energy has triggered great interest in the research and development of solar energy related science and technologies.[1−3] Photoelectrochemical (PEC) hydrogen production based on photoelectrodes, a promising and environmentally benign method for solar hydrogen generation, has attracted significant attention.[4−8] The commercialization of hydrogen fuel cell motors, for example, Toyota Mirai, will stimulate the clean hydrogen production based on solar energy, which is a totally clean route unlike the cracking of petroleum and natural gases. Hydrogen production on photocatalytic panels under concentrated solar radiation has proved to be competitive by National Renewable Energy Laboratory (NREL) of USA.[9] A self-driven tandem photoelectrode, which has cost advantage over single photoelectrodes working under applied bias, consists of a photocathode and a photoanode, which collect electrons and hole for surface hydrogen and oxygen reactions, respectively, in the case of direct water splitting.[9] Compared to photoanode materials, which are generally chemical stable oxides, the efficient photocathode materials, such as InP,[10] Cu_2O,[11] and Si,[3] all have the issue of chemical stability. The developing of efficient and stable photocathode is therefore critical for PEC devices. Silicon is the second most abundant element in the earth's crust with a narrow band gap (E_g = 1.1 eV), which is widely applied as photovoltaic materials and proved to be efficient as photoelectrodes for solar hydrogen production.[12−15] However, the surface reflection (~25%) of solar radiation[16] and the potential photocorrosion during PEC reaction, especially under concentrated radiation, remains an issue for Si photoelectrodes. Introduction of surface nanostructures and surface passivation layers significantly improve the solar absorption efficiency and chemical stability of many photoelectrodes.[3,12,17,18]

One dimensional Si nanowire arrays (NWAs) have received considerable attention due to its excellent optical absorption and the facilitated surface catalytic reaction. Various preparation methods have been utilized to produce surface nanowires, among which metal-assisted chemical etching (MACE) is one of the most economical and convenient methods due to its feasibility with low equipment requirement and adaptability for industrial fabrication.[19−21]

To improve the Si photoelectrode's long-term stability in aqueous environments, a variety of materials have been used to passive the surface, including metal,[12] metal oxide,[3] and conducting polymers.[22] TiO_2 is a good passivation material for surface protection of photoelectrodes because of its good electronic conductivity and chemical stability.[3,17,23] To lower the overpotential for hydrogen production, metal catalysts are usually deposited on the surface of photoelectrodes to catalyze the hydrogen production reaction. However, surface catalyst is supposed to work with direct contact to both the semiconductor and the electrolyte, which causes a puzzle when a surface passivation layer is also introduced. For application of chemically unstable semiconductors in PEC reactions, the configuration of the three components, semiconductor, catalyst, and the passivation layer, has to be figured out.

Amorphous TiO_2 has been proved to be a good conductor for photoelectrons and catalysts deposited on the surface of

Received: June 4, 2015
Accepted: August 11, 2015
Published: August 11, 2015

DOI: 10.1021/acsami.5b04936
ACS Appl. Mater. Interfaces 2015, 7, 18560−18565

TiO_2 have been shown to work well in photoelectrochemcial reactions.[3,24] Herein, we investigated the photocatalysis of Pt/Si with surface TiO_2 passivation layers, which stabilize both Si and the surface decorated Pt Nanoparticles. It is interesting that Pt nanoparticles buried underneath 15 nm TiO_2 layer still shows catalytic activity for hydrogen production without direct contact with electrolytes. The surface TiO_2 passivation layer not only conduct the catalytic effect of imbedded Pt nanoparticles, but stabilizes the composite photoelectrode in 0.5 M H_2SO_4 solution.

EXPERIMENTAL SECTION

Si Nanowire Array Fabrication. In this work, boron-doped P-type silicon wafers (with resistivity of 0.01−1 Ωcm) with crystal orientation of (100) were used. First, the wafer was cut into small chips (1 × 2 cm). All of the foils were degreased by sonication in acetone, ethanol, and deionized water, respectively. The Si chips were immersed in a solution of H_2SO_4/H_2O_2 with a volume ratio of 3:1 for 10 min. Then the samples were thoroughly rinsed with deionized water and dipped into a solution of HF. After that, they were immersed in an aqueous solution of 0.04 M silver nitrate ($AgNO_3$) and 4.6 M hydrofluoric acid (HF) for 20 s to deposit silver nanoparticles at 50 °C. Subsequently, the silicon chips were immersed in the etching solution composed of 4.6 M HF and 0.6 M hydrogen peroxide (H_2O_2) for 1 min. Finally, the Ag nanoparticles were removed by immersing the samples into aqua fortis for 15 min.

Pt Nanoparticles Deposition. For decoration of Pt nanoparticles onto Si nanowire arrays, the etched Si chips were first immersed in 0.4 M HF for 3 min to remove surface oxide. Then the samples were immersed into a solution of 0.4 M HF and 1 mM K_2PtCl_6 for 3 min, rinsing with DI water, and drying with N_2 flow.

Atomic Layer Deposition (ALD) of TiO_2. The as-prepared Si chips were then dipped in 5% HF solution for 10 min to completely remove the surface oxide layer, and then transferred to chamber of atomic layer deposition system (Ultratech, Savannah 100, USA), which was preheated to 150 °C. The deposition was performed with cycles of tetrakis-dimethylamino titanium (TDMAT, 0.1 s pulse), N_2 purges (20 s), and water vapor (0.015 s pulse).

Ohmic Contact Formation of the Samples. On the back side of the Si chip, an Ohmic contact was established by embedding a Cu wire in a eutectic gallium−indium alloy. The Cu wire and the eutectic were subsequently covered with silver paint. The epoxy was used to insulate the entire back side of the electrode and the Cu wire from the electrolyte. An area of 1 cm^2 on the front side of the Si electrode was exposed.

Characterization. The morphologies of the as-prepared samples were observed using a field-emission scanning electron microscope (FESEM, FEI, Sirion 200) and transmission electron microscope (TEM, JEM-2010HT). The sample for TEM was prepared by scratching off the powders from Si nanowire sample and dispersed in methanol solution, which was then dropped on carbon filaments suppoted by copper grid. Surface roughness of silicon wafer after long-term PEC reaction was studied using Atomic Force Microscopy (AFM) on a MultiMode 8 (Bruker) in scanasyst mode. The absorption properties of the samples were recorded using a reflectance UV−vis spectrometer (UV-3600, SHIMADZU). ICP measurements were performed on iCAP 6000 Radial (THERMO). X-ray photoelectron spectroscopic (XPS) measurements were performed on a Kratos AXIS Ultra DLD spectrometer.

Photoelectrochemical Measurements. All PEC measurements were carried out using CHI 660D electrochemical workstation in a standard three electrode configuration with a platinum wire as the counter electrode, a saturated calomel electrode (SCE) as the reference electrode, and the as-prepared samples as the working electrode. 0.5 M H_2SO_4 was used as the electrolyte. The illumination of 1 sun and 3 sun were provided by 300 W xenon lamp with AM 1.5 filter. The Faradaic efficiency was measured by collecting the evolved gas from the working electrode and comparing with the gas volume calculated based on the integral of observed photocurrent over illumination time. The IPCE (incident photon-to-current conversion efficiency) of the photoelectrode was measured under monochromatic illumination provided by SM-250 Hyper Monolight System (Bunkoukeiki, Japan).

RESULTS AND DISCUSSION

The Si nanowire based sandwich structure, TiO_2/Pt/SiNW, was obtained by facile wet deposition of Pt nanoparticles (Pt NPs) on the surface of p-Si nanowire arrays, which was prepared by Ag NPs catalyzed etching, and further passivated by amorphous TiO_2 layer by ALD technique. The structure of the TiO_2/Pt/SiNW photoelectrode is schematically presented in Figure 1a. The average length of the nanowire arrays are

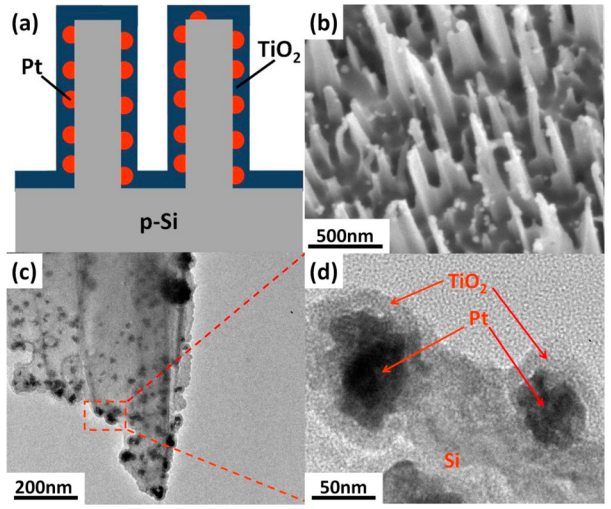

Figure 1. (a) Schematic, (b) SEM, and (c, d) TEM morphologies of the TiO_2/Pt/SiNW photoelectrode.

~450 nm and the diameter of the obtained wires is ~70 nm. Pt nanoparticles deposited through wet impregnation show sizes of 10−50 nm, as shown in Figure 1b, the top view of the as constructed sandwich structure, TiO_2/Pt/SiNW. Pt nanoparticles are imbedded between silicon nanowires and the surface TiO_2 passivation layer. This configuration is confirmed by the TEM images of the obtained powders scratched from the electrode, Figure 1c and 1d. According to the TEM images, the Pt particles are fully covered by TiO_2 layer with no direct contact with the surface electrolyte when applied in PEC reaction. The as deposited TiO_2 layer is ~15 nm.

Nanowire arrays have a better optical absorption than the planar silicon because of their specific morphology, which is consistent with the black appearance of the nanowire photoelectrodes instead of a mirror-like surface as in the untreated planar silicon wafer. This difference in optical absorption is confirmed by their UV−vis diffuse reflection spectra, Figure 2. The reflectance of TiO_2/Pt/SiNW sample is drastically reduced comparing to the planar Si. The superior antireflection properties of the TiO_2/Pt/SiNW can be attributed to the parallel wires that enable strong light trapping and scattering, which leads to improvement in light harvesting.[17]

The PEC performance of TiO_2/Pt/SiNW sandwich structure, Pt/SiNW, and planar Si are presented in Figure 3a. TiO_2/Pt/SiNW shows similar performance to Pt/SiNW in $I-V$ measurement with a slightly higher plateau photocurrent, which

DOI: 10.1021/acsami.5b04936
ACS Appl. Mater. Interfaces 2015, 7, 18560−18565

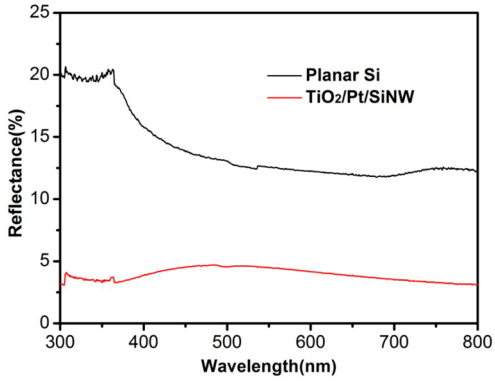

Figure 2. UV–vis reflection spectra of planar Si and TiO_2/Pt/SiNW photoelectrode.

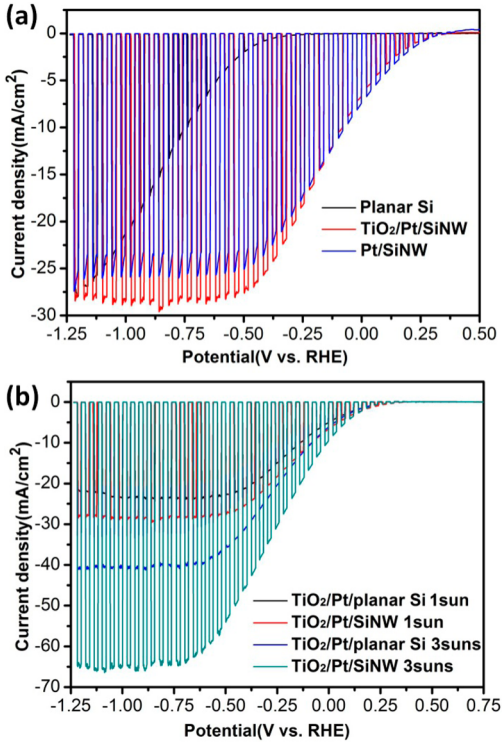

Figure 3. (a) Chopped I–V curves of planar Si, Pt/SiNW and TiO_2/Pt/SiNW photoelectrode, and (b) chopped I–V curves of TiO_2/Pt/planar Si and TiO_2/Pt/SiNW photoelectrode under 1 and 3 suns irradiation, measured in 0.5 M H_2SO_4 solution.

indicates that the passivation of Pt/SiNW by TiO_2 layer improves the performance. At an applied bias of −0.5 V_{RHE}, the photocurrent of the TiO_2/Pt/SiNW reaches −27 mA/cm^2, for which the bare Si wafer needs an applied bias of −1.25 V_{RHE}, Figure 3a. The photocurrent plateau is comparable with the −27 mA/cm^2 reported by Oh et al.[25] The photocurrent at 0 V_{RHE} is ∼7 mA/cm^2, which is also comparable with the p-Si/Pt wire array report by Lewis[18] and p-Si/Pt nanowire array with Pt by ALD reported by Yang.[26] The photocurrent at 0 V_{RHE} also suggests a good candidate of TiO_2/Pt/SiNW as the cathodic part of a tandem cell for self-driven water splitting.[27]

The onset potentials of TiO_2/Pt/SiNW and Pt/SiNW are both anodically shifted by 0.65 V relative to the bare planar Si. This clearly shows that the Pt nanoparticles in TiO_2/Pt/SiNW, which are physically isolated from the electrolyte by surface TiO_2 layer, catalyze the surface hydrogen production, as well as those in Pt/SiNW, which directly contact the electrolyte. It is interesting that the catalytic effect of the imbedded Pt nanoparticles can by conducted to the liquid–solid surface through the TiO_2 passivation layer. The TiO_2 layer prepared by ALD has been reported to have pinholes that might allow electrolyte to contact the inner Pt nanoparticles. However, due to the extremely small size of the pinholes, if present, and the large photocurrent density (−27 mA/cm^2) in our case, the catalysis reaction will face serious mass transfer limit and have significant decrease in the photocurrent density in a short time. However, a continuous photocurrent of −27 mA/cm^2 is observed in 2 h without obvious degradation, Figure 4a. Therefore, the pinholes should not be main reason for the catalytic effect. The photoelectrons concentrated on Pt nanoparticles from the silicon substrate thus "tunnel" through the TiO_2 layer to the electrolyte and reduce protons into hydrogen without significant overpotential. It seems like the catalytic effect of the imbedded Pt particles can be conducted by the TiO_2 layer to the solid/liquid junction, as schematically shown in Figure S1. When an additional thin layer of Al_2O_3 (0.2 nm), which was reported to be condense without pinholes,[11] was deposited before TiO_2 deposition on Si/Pt, the composite TiO_2/Al_2O_3/Pt/Si shows similar onset potential and PEC performance under the same conditions, Figure S2. This further confirms the tunnelling mechanism of the surface catalysis instead of pinholes. The electronic tunnelling could be attributed to the good electronic conductivity of amorphous TiO_2 prepared by ALD, which allows the passage of very high (>1 A cm^{-2}) current densities as a "leaky" dielectric.[3] The mechanism of the catalytic conducting however awaits further investigation. The thickness of TiO_2 layer was investigated on the catalytic activity of the imbedded Pt on planar Si by increasing the ALD deposition cycles of TiO_2 from 125 cycles to 500 cycles, which corresponds to a thickness increase from ∼15 to ∼60 nm. The TiO_2 layer of 250 cycles shows almost the same PEC performance with the 125 cycles, while the onset potential shifts cathodically by 0.1 V for the sample with 500 cycles, Figure S3. Therefore, a passivation layer of TiO_2 with thickness of no more than 30 nm will have similar catalytic effect on hydrogen production.

Under 1 sun illumination, the TiO_2/Pt/SiNW shows only slight advantage in PEC performance over the TiO_2/Pt/planar Si. The plateau photocurrent density of TiO_2/Pt/SiNW is −27 mA/cm^2 and that of TiO_2/Pt/planar Si is −23 mA/cm^2, as shown in Figure 3b. When the illumination density is increased to 3 sun, the photocurrent density of the planar photoelectrode increases to −40 mA/cm^2, which is ∼1.7 times increase. The current density for the nanowire electrode increases from −27 mA/cm^2 to −65 mA/cm^2 under 3 sun illumination, which is ∼2.4 times increase, as shown in Figure 3b. The nanowire photoelectrodes therefore performs much better than the planar one under more intensive solar radiation. This could be attributed to the higher optical absorption efficiency and faster hydrogen bubbling kinetics.[28,29] The difference in bubbling kinetics is also observed by the size of the hydrogen bubbles on the planar and nanowire silicon photoelectrodes, Figure 4b. The efficiency of TiO_2/Pt/SiNW under concentrated illumination is still lower than that under the standard 1 sun illumination. This could probably be due to the mass transfer limit of the electrolytes because of the high consumption rate of the surface protons and the limited evolution speed of the hydrogen gas. Longer wires and smaller Pt nanoparticle would

DOI: 10.1021/acsami.5b04936
ACS Appl. Mater. Interfaces 2015, 7, 18560–18565

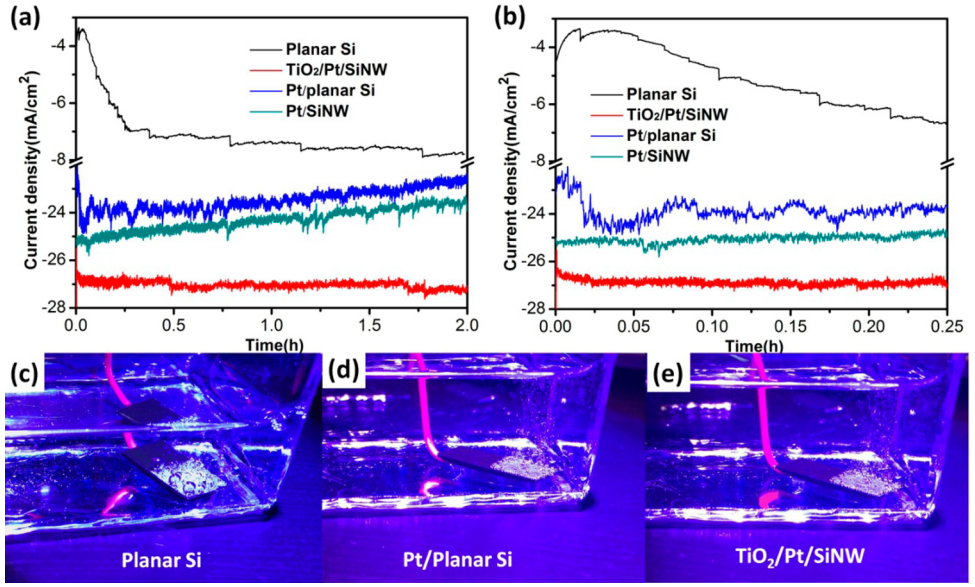

Figure 4. (a) Chemical stability test on the photoelectrochemical reaction of the bare planar Si, Pt/planar Si, Pt/SiNW and TiO_2/Pt/SiNW samples in H_2SO_4 (0.5M) under 100 mW/cm^2 illumination. The applied potential was −0.5 V (vs RHE). (b) Partial details of the curves in (a). (c, d, e) Optical pictures depicting the effect of H_2 bubble formation on the surfaces of the planar Si, Pt/planar Si and TiO_2/Pt/SiNW samples, respectively, during PEC measurements under 1 sun illumination.

further improve the performance under concentrated illumination.

The chemical stability of the photoelectrode is characterized by the continuous 2h PEC experiments. The photocurrents of the bare planar Si electrode, the Pt planar/Si electrode, Pt/SiNW and the TiO_2/Pt/SiNW electrode in H_2SO_4 (0.5 M) under 100 mW/cm^2 illumination and applied bias of −0.5 V_{RHE} are shown in Figure 4. The initial photocurrent of planar Si sample is ∼−4.5 mA/cm^2, which is consistent to the result of I−V curve in Figure 3a. However, the recorded photocurrent density increased to ∼8 mA/cm^2 after 2 h. This should be due to the corrosion of surface Si metals and the resultant increase of the surface roughness/nanostructure that enhances the optical absorption and accelerates photoelectrochemical reaction. The AFM characterization (Figure S4) observed a higher surface roughness of planar Si sample after 2 h PEC reaction. The XPS spectra of the Si 2p region of planar Si before and after 2h stability test are shown in Figure S5. The result shows an obvious increase of Si^{4+} after 2h PEC reaction, which can be attributed to the increase of the surface thickness of SiO_2 layer. Since there is no change of the Si concentration in the electrolyte from ICP study, we suspect that the photocorrosion does not experience dissolution of the Si metal in the solution. The corrosion directly lead to the formation of SiO_2 layer on the surface active sites resulting in increase of surface roughness. With surface decoration of Pt nanoparticles, the planar silicon electrode shows a significantly increased photocurrent from −4.5 to −24 mA/cm^2, which suggests a crucial role of the Pt catalyst in the PEC performance of silicon photoelectrodes. This indicates that the quick consumption of photogenerated electrons on the surface significantly decrease the electron-pair recombination opportunity. Instead of current density increase in the case of bare Si electrode, the Pt/planar Si and Pt/SiNW sample both show a continuous decline in the photocurrent. This should be partially ascribed to the corrosion of surface Si metal and the resultant desorption of Pt nanoparticles from the surface. The TiO_2/Pt/SiNW, on the contrary, shows a stable cathodic photocurrent of approximately −27 mA/cm^2 throughout the 2 h test. It is obvious that TiO_2 passivation layer effectively stabilize Pt/SiNW composite electrode from photochemical corrosion.

The fluctuations in the photocurrent density is closely related to the bubbling of hydrogen. Figure 4b shows the enlarged detail of the chemical stability test. The sharp fluctuations of photocurrent curve of the bare Si electrode could be attributed to the formation and release of big H_2 bubbles on planar wafer, as shown in Figure 4c. In contrast, Pt/planar Si, Pt/SiNW and TiO_2/Pt/SiNW samples all show stable photocurrent with relatively smooth curve. Small H_2 bubbles are observed on both the "black" Si wafer surface and Pt decorated planar Si wafer, which confirm the easier evolution of smaller H_2 bubbles on nanowires and/or the presence of Pt, as shown in Figure 4d and Figure 4e. Larger H_2 bubbles will occupy the surface of photoelectrode and interfere the diffusion of electrolytes, which leads to a slower surface catalytic reaction and accumulation of surface photoelectrons. In contrast, H_2 gas bubbles do not stick to the surface of the TiO_2/Pt/SiNW and desorb quickly from the surface owing to the low surface energy of the TiO_2/Pt/SiNW sample (Figure 4e).[10] The Pt/planar Si sample also shows fast bubbling kinetics because of the catalytic effect of Pt nanoparticles, however, the small surface area of the planar wafer also limit the bubbling kinetics and cause a relatively bigger fluctuation of the current curve than the nanowire electrodes, as shown in Figure 4d, which indicates the advantage of nanowire morphology on the evolution of hydrogen gas bubbles.

The overall PEC performance was evaluated by computing the photon-to-energy conversion efficiency of the PEC cell (η_{cell}) according to the following equation,[30]

$$\eta_{cell} = \frac{I_p(V_{rev}^0 - |V_{meas} - V_{aoc}|)}{P_t} \quad (1)$$

where I_p is the photocurrent density, P_t is the power density of incident light (100 mW/cm^2 for this study), V_{rev}^0 = 1.23 V is the standard reversible potential, V_{meas} is electrode potential of the

DOI: 10.1021/acsami.5b04936
ACS Appl. Mater. Interfaces 2015, 7, 18560−18565

working electrode at which photocurrent is measured under illumination, and V_{aoc} is the electrode potential of the same working electrode at open circuit conditions under same illumination and in the same electrolyte. The calculated results are shown in Figure 5. The maximum H_2 production efficiency

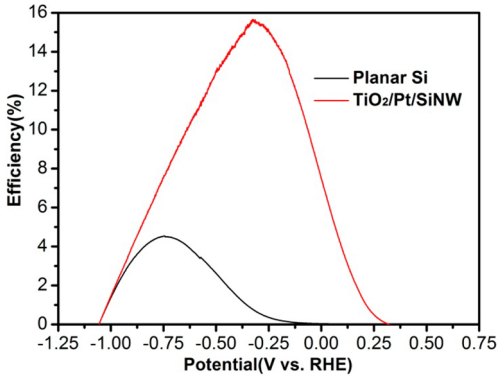

Figure 5. Energy conversion efficiency as a function of applied bias.

of TiO_2/Pt/SiNW photoelectrode is approximately 15.6% at an applied bias of −0.32 V_{RHE}. This efficiency value is much higher than the planar Si sample (4.5%) measured using the same setup. The efficiency at 0 V_{RHE} reaches 8%, which is close to the industrial target (10%) for photocatalytic energy production.[9] The IPCE of the TiO_2/Pt/SiNW photoelectrode at −0.5 V_{RHE}, Figure S6, shows a maximum conversion efficiency of ∼76% at 700 nm, which is comparable with the reports by Jun.[31] The Faradaic efficiency, which is ∼100%, was also measured by comparing the volume of the evolved H_2 to the calculated one based on the observed cathodic current, Figure S7.

CONCLUSIONS

In summary, Si nanowire arrays decorated with Pt nanoparticles and fully passivated with amorphous TiO_2 layer by ALD shows superior photoelectrochemical performance to the planar Si, Pt/planar Si, and TiO_2/Pt/planar Si photoelectrodes in terms of chemical stability and photoresponse under 1 sun and concentrated illumination. The maximum cathodic photocurrent of the TiO_2/Pt/SiNW is ∼−27 mA/cm^2 under 100 mW/cm^2 illumination and −65 mA/cm^2 under 300 mW/cm^2 illumination. The onset potential on the TiO_2/Pt/SiNW sample is 0.35 V_{RHE} and the maximum photon-to-energy conversion efficiency of the TiO_2/Pt/SiNW sample is 15.6%.

ASSOCIATED CONTENT

Supporting Information

The Supporting Information is available free of charge on the ACS Publications website at DOI: 10.1021/acsami.5b04936.

Schematic process of the "tunneling" of Pt catalytic effect through TiO_2 passivation layer to liquid−solid interface for hydrogen production, chopped I−V curves of TiO_2/Al_2O_3/Pt/SiNW photoelectrode, photocurrent curves of planar Si, Pt/planar Si with 125, 250, and 500 cycles TiO_2, AFM images, XPS, IPCE, and hydrogen evolution results (PDF)

AUTHOR INFORMATION

Corresponding Authors

*E-mail: pengzhang2010@sjtu.edu.cn.

*E-mail: liangao@mail.sic.ac.cn.

Notes

The authors declare no competing financial interest.

ACKNOWLEDGMENTS

The authors greatly acknowledge the financial support by the National Natural Science Foundation of China (*No.*51172142, 51302169), Shanghai Municipal Natural Science Foundation (*No.*12ZR1414300), and the Third Phase of 211 Project for Advanced Materials Science (*No.* WS3116205007). This research is also supported by the Opening Project of State Key Laboratory of High Performance Ceramics and Superfine Microstructure (SKL201305SIC). The authors also thank Prof. Liyuan Han, Dr. Han Chen, and Prof. Tao Deng for discussion and support in characterizations.

REFERENCES

(1) Zhang, P.; Gao, L.; Song, X.; Sun, J. Micro- and Nanostructures of Photoelectrodes for Solar-Driven Water Splitting. *Adv. Mater.* **2015**, *27*, 562−568.

(2) Fujishima, A.; Honda, K. Electrochemical Photolysis of Water at a Semiconductor Electrode. *Nature* **1972**, *238*, 37−38.

(3) Hu, S.; Shaner, M. R.; Beardslee, J. A.; Lichterman, M.; Brunschwig, B. S.; Lewis, N. S. Amorphous TiO_2 Coatings Stabilize Si, GaAs, and GaP Photoanodes for Efficient Water Oxidation. *Science* **2014**, *344*, 1005−1009.

(4) Li, S.; Zhang, P.; Song, X.; Gao, L. Ultrathin Ti-doped Hematite Photoanode by Pyrolysis of Ferrocene. *Int. J. Hydrogen Energy* **2014**, *39*, 14596−14603.

(5) Zhang, P.; Kleiman-Shwarsctein, A.; Hu, Y. S.; Lefton, J.; Sharma, S.; Forman, A. J.; McFarland, E. Oriented Ti Doped Hematite Thin Film as Active Photoanodes Synthesized by Facile APCVD. *Energy Environ. Sci.* **2011**, *4*, 1020−1028.

(6) Wang, X.; Peng, K. Q.; Hu, Y.; Zhang, F. Q.; Hu, B.; Li, L.; Wang, M.; Meng, X. M.; Lee, S. T. Silicon/Hematite Core/Shell Nanowire Array Decorated with Gold Nanoparticles for Unbiased Solar Water Oxidation. *Nano Lett.* **2014**, *14*, 18−23.

(7) Wu, J.; Li, Y.; Kubota, J.; Domen, K.; Aagesen, M.; Ward, T.; Sanchez, A.; Beanland, R.; Zhang, Y.; Tang, M.; Hatch, S.; Seeds, A.; Liu, H. Wafer-Scale Fabrication of Self-Catalyzed 1.7 eV GaAsP Core−Shell Nanowire Photocathode on Silicon Substrates. *Nano Lett.* **2014**, *14* (4), 2013−2018.

(8) Hu, S.; Chi, C. Y.; Fountaine, K. T.; Yao, M.; Atwater, H. A.; Dapkus, P. D.; Lewis, N. S.; Zhou, C. Optical, Electrical, and Solar Energy-Conversion Properties of Gallium Arsenide Nanowire-Array Photoanodes. *Energy Environ. Sci.* **2013**, *6* (6), 1879−1890.

(9) Turner, J. A. Shining a Light on Solar Water Splitting Response. *Science* **2014**, *344*, 469−470.

(10) Lee, M. H.; Takei, K.; Zhang, J.; Kapadia, R.; Zheng, M.; Chen, Y. Z.; Nah, J.; Matthews, T. S.; Chueh, Y. L.; Ager, J. W.; Javey, A. P-Type InP Nanopillar Photocathodes for Efficient Solar-Driven Hydrogen Production. *Angew. Chem., Int. Ed.* **2012**, *51* (43), 10760−10764.

(11) Paracchino, A.; Laporte, V.; Sivula, K.; Grätzel, M.; Thimsen, E. Highly Active Oxide Photocathode for Photoelectrochemical Water Reduction. *Nat. Mater.* **2011**, *10* (6), 456−461.

(12) Kenney, M. J.; Gong, M.; Li, Y.; Wu, J. Z.; Feng, J.; Lanza, M.; Dai, H. High-Performance Silicon Photoanodes Passivated with Ultrathin Nickel Films for Water Oxidation. *Science* **2013**, *342* (6160), 836−840.

(13) Qi, X.; She, G.; Huang, X.; Zhang, T.; Wang, H.; Mu, L.; Shi, W. High-Performance n-Si/α-Fe_2O_3 Core/Shell Nanowire Array Photoanode towards Photoelectrochemical Water Splitting. *Nanoscale* **2014**, *6* (6), 3182−3189.

(14) Hwang, Y. J.; Wu, C. H.; Hahn, C.; Jeong, H. E.; Yang, P. Si/InGaN Core/Shell Hierarchical Nanowire Arrays and their Photoelectrochemical Properties. *Nano Lett.* **2012**, *12* (3), 1678−1682.

DOI: 10.1021/acsami.5b04936
ACS Appl. Mater. Interfaces 2015, 7, 18560−18565

(15) Hou, Y.; Abrams, B. L.; Vesborg, P. C. K.; Bjorketun, M. E.; Herbst, K.; Bech, L.; Setti, A. M.; Damsgaard, C. D.; Pedersen, T.; Hansen, O.; Rossmeisl, J.; Dahl, S.; Norskov, J. K.; Chorkendorff, I. Bioinspired Molecular Co-Catalysts Bonded to a Silicon Photocathode for Solar Hydrogen Evolution. *Nat. Mater.* **2011**, *10* (6), 434−438.
(16) Oh, J. H.; Deutsch, T. G.; Yuan, H. C.; Branz, H. M. Nanoporous Black Silicon Photocathode for H_2 Production by Photoelectrochemical Water Splitting. *Energy Environ. Sci.* **2011**, *4* (5), 1690−1694.
(17) Huang, S.; Zhang, H.; Wu, Z.; Kong, D.; Lin, D.; Fan, Y.; Yang, X.; Zhong, Z.; Huang, S.; Jiang, Z.; Cheng, C. Large-Area Ordered P-type Si Nanowire Arrays as Photocathode for Highly Efficient Photoelectrochemical Hydrogen Generation. *ACS Appl. Mater. Interfaces* **2014**, *6* (15), 12111−12118.
(18) Boettcher, S. W.; Warren, E. L.; Putnam, M. C.; Santori, E. A.; Turner-Evans, D.; Kelzenberg, M. D.; Walter, M. G.; McKone, J. R.; Brunschwig, B. S.; Atwater, H. A.; Lewis, N. S. Photoelectrochemical Hydrogen Evolution Using Si Microwire Arrays. *J. Am. Chem. Soc.* **2011**, *133* (5), 1216−1219.
(19) Huang, Z.; Zhang, X.; Reiche, M.; Liu, L.; Lee, W.; Shimizu, T.; Senz, S.; Gösele, U. Extended Arrays of Vertically Aligned Sub-10 nm Diameter [100] Si Nanowires by Metal-Assisted Chemical Etching. *Nano Lett.* **2008**, *8* (9), 3046−3051.
(20) Peng, K.; Xu, Y.; Wu, Y.; Yan, Y.; Lee, S. T.; Zhu, J. Aligned Single-Crystalline Si Nanowire Arrays for Photovoltaic Applications. *Small* **2005**, *1* (11), 1062−1067.
(21) Peng, K.; Lu, A.; Zhang, R.; Lee, S. T. Motility of Metal Nanoparticles in Silicon and Induced Anisotropic Silicon Etching. *Adv. Funct. Mater.* **2008**, *18* (19), 3026−3035.
(22) Li, X.; Lu, W.; Dong, W.; Chen, Q.; Wu, D.; Zhou, W.; Chen, L. Si/PEDOT Hybrid Core/Shell Nanowire Arrays as Photoelectrodes for Photoelectrochemical Water-Splitting. *Nanoscale* **2013**, *5* (12), 5257−5261.
(23) Seger, B.; Pedersen, T.; Laursen, A. B.; Vesborg, P. C. K.; Hansen, O.; Chorkendorff, I. Using TiO_2 as a Conductive Protective Layer for Photocathodic H_2 Evolution. *J. Am. Chem. Soc.* **2013**, *135* (3), 1057−1064.
(24) Shaner, M. R.; Hu, S.; Sun, K.; Lewis, N. S. Stabilization of Si Microwire Arrays for Solar-Driven H_2O Oxidation to O_2(g) in 1.0 M KOH(aq) using Conformal Coatings of Amorphous TiO_2. *Energy Environ. Sci.* **2015**, *8* (1), 203−207.
(25) Oh, I.; Kye, J.; Hwang, S. Enhanced Photoelectrochemical Hydrogen Production from Silicon Nanowire Array Photocathode. *Nano Lett.* **2012**, *12* (1), 298−302.
(26) Dasgupta, N. P.; Liu, C.; Andrews, S.; Prinz, F. B.; Yang, P. Atomic Layer Deposition of Platinum Catalysts on Nanowire Surfaces for Photoelectrochemical Water Reduction. *J. Am. Chem. Soc.* **2013**, *135* (35), 12932−12935.
(27) Sun, K.; Shen, S.; Liang, Y.; Burrows, P. E.; Mao, S. S.; Wang, D. Enabling Silicon for Solar-Fuel Production. *Chem. Rev.* **2014**, *114* (17), 8662−8719.
(28) Chen, R.; Lu, M. C.; Srinivasan, V.; Wang, Z.; Cho, H. H.; Majumdar, A. Nanowires for Enhanced Boiling Heat Transfer. *Nano Lett.* **2009**, *9* (2), 548−553.
(29) Li, C.; Wang, Z.; Wang, P. I.; Peles, Y.; Koratkar, N.; Peterson, G. P. Nanostructured Copper Interfaces for Enhanced Boiling. *Small* **2008**, *4* (8), 1084−1088.
(30) Varghese, O. K.; Grimes, C. A. Appropriate Strategies for Determining the Photoconversion Efficiency of Water Photo Electrolysis Cells: A Review with Examples using Titania Nanotube Array Photoanodes. *Sol. Energy Mater. Sol. Cells* **2008**, *92* (4), 374−384.
(31) Jun, K.; Lee, Y. S.; Buonassisi, T.; Jacobson, J. M. High Photocurrent in Silicon Photoanodes Catalyzed by Iron Oxide Thin Films for Water Oxidation. *Angew. Chem.* **2012**, *124* (2), 438−442.

DOI: 10.1021/acsami.5b04936
ACS Appl. Mater. Interfaces 2015, 7, 18560−18565